

Time-Dependent Photoionization in a Dusty Medium II: Evolution of Dust Distributions and Optical Opacities

Rosalba Perna^{1,2}, Davide Lazzati³ and Fabrizio Fiore⁴

ABSTRACT

The interaction of a radiation field with a dusty medium is a relevant issue in several astrophysical contexts. We use the time-dependent photoionization code in a dusty medium developed by Perna & Lazzati (2002), to study the modifications in the dust distribution and the relative optical opacities when a strong X-ray UV radiation flux propagates into a medium. We find that silicates are preferentially destroyed with respect to graphite, and the extinction curve becomes significantly flatter (hence implying less reddening), with the characteristic bump at λ 2175 Å highly suppressed, due to the destruction of the small graphite grains. This could explain the observational lack of such a feature in GRB afterglow and AGN spectra. For a very intense and highly variable source irradiating a compact and dense region, time variability in the optical opacity resulting from dust destruction can be observed on a relatively short timescale. We show that, under these circumstances, monitoring the time variability of the opacity can yield powerful clues on the properties of dust in the environment of the source. In particular, it allows to break the observational degeneracy as to whether a grey extinction is the result of a low dust-to-gas ratio or of a dust grain distribution that is skewed towards large grains.

Subject headings: dust, extinction — galaxies: ISM

1. Introduction

The effects of the interaction between a strong radiation field and a dusty environment are of relevance in several astrophysical contexts, most notably Active Galactic Nuclei (AGNs), Gamma-Ray Bursts (GRBs) and star formation (SF). The radiation field can significantly alter the properties of the dust in the close environment of the source, producing effects that, for a time-variable and intense source, can be observable on a very short time scale. When time

¹Harvard Society of Fellows, 74 Mount Auburn Street, Cambridge, MA 02138

²Harvard-Smithsonian Center for Astrophysics, 60 Garden Street, Cambridge, MA 02138

³Institute of Astronomy, University of Cambridge, Madingley Road, Cambridge CB3 0HA, UK

⁴Osservatorio Astronomico di Roma, via dell'Osservatorio, 2, I-00040, Monte Porzio Catone, Roma, Italy

variability of the opacities is indeed observed, a great deal of information can be gained on the properties of the dusty cloud which is being irradiated. This is for example the case of GRBs, where time variability in absorption lines (Perna & Loeb 1998; Böttcher et al. 1999; Mirabal et al. 2002), in X-ray opacity (Lazzati et al. 2001a, Lazzati & Perna 2002), and in optical extinction (Waxman & Draine 2000; Draine & Hao 2002; Perna & Lazzati 2002), have been proposed and used (Amati et al. 2000; Lazzati et al. 2001b) to learn about the properties of the close GRB environment. And it should be noted that the nature of the GRB environments is a particularly important issue not only because the type of environment in which GRBs occur can be a strong diagnostic of the GRB progenitors, but more generally because GRBs probe inner regions of galaxies, not accessible to QSO absorption studies. Therefore they constitute an invaluable complement to QSO absorption studies in order to have a fair idea of what the properties of high-redshift galaxies are. To this purpose, it is particularly important to have a proper estimate of metallicity and dust content (i.e. dust-to-gas ratio).

The properties of dust in the close environment of AGNs appear somewhat anomalous and, in general, different than the Galactic ones. Laor & Draine (1993) note how spectral observations suggest that silicates are highly depleted with respect to graphite, and/or dust must be composed of grains larger than the typical grains in the Galaxy. Similar conclusions on the presence of a dust distribution which is skewed towards large grains has also been reached by Maiolino et al. (2001a; see however Weingartner & Murray 2002), whose analysis includes measurements of reddening for a large sample of AGNs and comparison with the Galactic value.

In the case of GRBs, measurements of dust properties have yielded so far results that may appear contradictory: Savaglio, Fall & Fiore (2002) find a dust-to-gas ratio in GRB spectra that is higher than in QSO-selected DLAs and generally consistent with the solar value, while Wijers & Galama (2000), based on an analysis of the reddening in the afterglow spectra (and using a Galactic-type extinction curve) infer a dust-to-gas ratio that is much lower than the Galactic value. A way to reconcile the two types of observations can be the presence of a dust grain distribution that is skewed towards larger grains (e.g. Stratta et al. 2002), similarly to what inferred for AGNs. As far as extinction is concerned, a Galactic-type grain distribution with a low dust-to-gas ratio can yield the same extinction of a grain distribution that is skewed towards larger grains, but for which the dust-to-gas ratio is larger.

In this paper we discuss the shape and composition of the dust distribution left behind by a strong and variable source of ionizing photons, as well as the evolution of the extinction during the destruction phase. We will show that, since small grains can be more easily destroyed by the interaction with the photons, and since graphite particles are more resistant to destruction, the typical outcome is a dust distribution skewed towards big graphite particles. Such a result may explain the observational findings of Laor & Draine (1993) and Maiolino et al. (2001a). In order to test such speculations, we suggest to use, as sources, the very early afterglows of GRBs. In these events, in fact, a virtually unperturbed cloud is suddenly illuminated by a strong photon flux, and the evolution of reddening and absorption may be followed through photometric

observations of the dedicated *Swift* satellite. We will show how monitoring the time evolution of the extinction allows to break the observational degeneracy as to whether a grey extinction is the result of a low dust-to-gas ratio or of a dust grain distribution that is skewed towards large grains. It should however be remarked that a significant (and therefore observable) time variability can only be observed for a source which irradiates a dense and compact region (e.g. Perna & Loeb 1998; Mirabal et al. 2002). For the case of GRBs, this should be possible in some cases, as there is evidence that at least a fraction of long GRBs are associated with the collapse of massive stars (Fruchter et al. 1999, Kulkarni et al. 1999), and therefore are expected to occur in dense and dusty environments as typical of star forming regions.

The paper is organized as follows: in §2, we discuss the theoretical modelling of the extinction curve and its observational characteristics as a function of the underlying dust grain distribution. In §3, we study the time evolution of the opacity under an intense radiation field in different types of dusty environments, including the influence on the opacity of the presence of Hydrogen in molecular form. The observational perspectives for detection of variability on a short time scale are discussed in §4. Finally, a summary is presented in §5.

2. Modelling the Evolution of the Dust Grain Distribution

2.1. Brief review of the code

The code which models the evolution of the dust grain distribution is described in detail in Perna & Lazzati (2002; Paper I in the following); here we only provide a brief summary. The code includes the destruction processes of dust due to UV and X-ray sublimation, as well as ion field emission⁵. It treats dust as a mixture of silicates and graphite (similarly to what inferred for Galactic-type dust; Mathis et al. 1977), and it follows the evolution of each of the two species. It allows for any initial grain-size distribution, and it follows its evolution in space and time. While following the evolution of the dust grains under the influence of the radiation field, the code also follows the evolution of Hydrogen (which can initially be in any mixture of its atomic and molecular phase), and the 12 most abundant astrophysical elements, using the photoionization routines described in Perna, Raymond & Loeb (2000). For the elements depleted into dust (i.e. C, Mg, Si, O, Fe), the abundances in the gaseous and in the dust-depleted phase are separately being kept track of, following the recycling from dust into gas as dust is being sublimated away.

⁵For heavily charged grains, the process of ion field emission (IFE) is in competition with the process of Coulomb explosion (CE) that results in grain fragmentation (Waxman & Draine 2000; Fruchter, Krolik & Rhoads 2001; Reichart 2001a). The importance of CE versus IFE is uncertain, as it depends on the not well known resistance of chemical bonds to disruption by a photoionization field (see Draine & Hao 2002 and Paper I for a more extended discussion). Here, as in Paper I, we assume that IFE is the dominant effect in highly charged grains. However, we envisage an observational test (see §4) that can help discriminate whether IFE or CE actually dominate.

2.2. Computation of the extinction curve

The dust extinction curve $A(\nu)$ in the region below 1.25 keV is computed in the code by interpolation using the tables⁶ provided by Draine and collaborators (Draine & Lee 1985; Laor & Draine 1993) for the coefficient of absorption $Q_{\text{abs}}(a, \nu)$, the coefficient of scattering $Q_{\text{sca}}(a, \nu)$, and the scattering asymmetry factor g . In terms of these quantities, the extinction in a region of radius R is given by

$$A(\nu) = \int_0^R dr \sum_{i=1}^2 \int da \pi a^2 \frac{dn_i(a)}{da} [Q_{\text{abs},i}(a, \nu) + (1-g)Q_{\text{sca},i}(a, \nu)] . \quad (1)$$

In the above equation, dn_i/da indicates the dust grain distribution, while the indices $i = 1, 2$ represent the two types of dust grains that we are considering here, i.e. silicate and graphite. For simplicity we assume that, prior to the onset of the source, the size distribution of the grains is a power law⁷

$$\frac{dn_i}{da} = A_i n_{\text{H}} a^{-\beta} \quad a_{\text{min}} \leq a \leq a_{\text{max}} . \quad (2)$$

For a given size distribution of the dust grains (characterized by the parameters a_{min} , a_{max} and β), the coefficients A_i can be related to the dust-to-gas ratio f_d (defined as the ratio between the total mass in dust and the total mass in hydrogen) through the relation

$$f_d \equiv \frac{m_{\text{dust}}}{m_{\text{Hyd}}} = \frac{4\pi}{3m_{\text{H}}} \frac{a_{\text{max}}^{4-\beta}}{(4-\beta)} \left[1 - \left(\frac{a_{\text{min}}}{a_{\text{max}}} \right)^{4-\beta} \right] \sum_i A_i \rho_i , \quad (3)$$

having assumed a spherical shape for the dust grains. The value $f_d \approx 0.01$ is typical of the solar neighborhood with the grain densities $\rho_{\text{Sil}} \approx 3.3 \text{ g cm}^{-3}$ and $\rho_{\text{Gra}} \approx 2.26 \text{ g cm}^{-3}$ (e.g. Draine & Lee 1984), respectively for silicates and graphite. We take the initial mass ratio between the two species of grains to be similar to the solar value

$$m_{\text{Gra}} = \frac{A_{\text{Gra}} \rho_{\text{Gra}}}{A_{\text{Sil}} \rho_{\text{Sil}}} \approx 0.88 . \quad (4)$$

Figure 1 shows the extinction curve constructed as described in Eq. (1), and using the grain distribution in Eq. (2) for the size range $a_{\text{min}} = 0.005 \mu\text{m}$, $a_{\text{max}} = 0.25 \mu\text{m}$, which best describes the Galactic absorption with a slope $\beta = 3.5$ (Mathis et al. 1977). The Galactic extinction curve (solid line) is compared in Figure 1 to extinction curves produced by shallower distributions of grains. As it can be seen, the shallower the grain size distribution, the flatter the extinction curve (and therefore the smaller the reddening). This is shown more clearly in Figure 2, where the extinction in the V band (top panel) and the B-V reddening (bottom panel) are shown as a function of β for three different values of the maximum size of the grain distribution a_{max} .

⁶They can be found at <http://astro.Princeton.EDU/~draine/dust/dust.html>.

⁷This is a good approximation for our Galaxy, while not much is known on the shape of the distribution in other galaxies.

2.3. Time evolution of the grain size distribution and extinction curve

As summarized in §2.1 (and described in great detail in Paper I), our code follows in space and in time the evolution of the grain distribution dn_i/da . An example is shown in Figure 3, where the shape of the grain distribution (for the silicates and the graphite separately) at some distance $r \sim 2 \times 10^{18}$ cm from the source is plotted at several times while the region is being illuminated by a source with spectrum $L_\nu \propto \nu^{-0.5}$ and normalization equal to 10^{50} erg/sec in the 1eV - 100keV range⁸. At $t = 0$, the (power-law) grain distribution has a slope $\beta = 3.5$ in the size range $\{0.005, 0.25\}$ μm . As grain destruction proceeds, the value of the largest grain in the distribution, a_{\max} , is being reduced. The grain distribution evolves as grains are being reduced in size, thus causing an increase in the density of particles of smaller size a . On the other hand, the smaller the grains, the more easily they are sublimated away, and therefore the low- a tail of the distribution evolves more rapidly. The overall effect of the time-evolution is a gradual flattening of the distribution and reduction of a_{\max} . It should also be noted that the grain distribution for the silicates evolves much more rapidly than that for graphite, which is harder to destroy (see also Paper I).

Figure 4 (top panel) shows the evolution of the extinction curve $A(\nu)$ for the same illuminating spectrum used in Figure 3, and for a region of size $R = 10^{19}$ cm and density $n = 10^3 \text{ cm}^{-3}$, with a dust-to-gas ratio equal to the solar value. The initial size distribution, $dn_i(r, t = 0)/da$, of the grains producing the extinction is also taken as in Figure 3, for all $r \leq R$. As grain destruction proceeds, the extinction curve becomes flatter, reflecting the shallower slope of the grain size distribution, as illustrated by Figure 3. Another important consequence of the modification in the grain size distribution is a significant reduction of the characteristic bump at $\lambda 2175 \text{ \AA}$ in the extinction curve. This bump is indeed found to be highly depleted in AGNs (see e.g. Maiolino et al. 2001b), and it has not been found in spectroscopic analysis of GRB light curves, even though the resolution should have been sufficient to detect it (Galama & Wijers 2001).

The bottom panel of Figure 4 shows the relative contribution to the opacity from graphite and silicates. Before the onset of the source, the dust mass in these two components is taken as for galactic-type dust (Mathis et al. 1977). However, it can be seen that, as the radiation flux impinges on the dust grains, the contribution to the opacity by silicates becomes negligible with respect to that by graphite. This is due to the shorter timescale for destruction of silicates (see Figure 3 and Paper I).

An important implication of this result in the context of GRBs occurring in dense and compact regions (only for these regions, we remark once again, dust can be significantly destroyed by the burst prompt emission) is that afterglow observations, which are made at later times, would

⁸It should be remarked that, unlike photoionization, for the purpose of dust destruction what matters is not only the fluence of the source, but also its luminosity. Therefore, for the same fluence, a source of shorter duration but higher luminosity is more effective to destroy dust than a less luminous but more longer-lived source. This is why the prompt emission of GRBs is so effective in destroying dust.

preferentially detect the absorption features in the spectra associated with graphite with respect to those associated with silicates. However, as the absorption features are mostly produced by small grains, and these are preferentially destroyed by the radiation also in the case of graphite, there will be an overall suppression of the absorption features associated with graphite as well (and this is exemplified by the suppression of the $\lambda 2175$ dust bump discussed above). More generally, our results imply that, in a dusty medium subject to an intense source of radiation, the properties of dust must be different than the Galactic one, in that the silicates should be depleted with respect to graphite. It should be noted that, for the spectrum assumed in this discussion, dust destruction is mainly due to thermal sublimation of the dust grains, heated by absorption of the UV continuum. Nevertheless, this result seems to be quite independent of the spectrum of the ionizing source, and holds even for an IFE dominated destruction (see Lazzati & Perna 2002, Paper 3).

We speculate that our results could help explain the unusual depletion of silicates with respect to graphite also in the environment of active galactic nuclei (e.g. Laor & Draine 1993). In the Maiolino et al. (2001a, 2001b) sample, the central source of photons has [2–10] keV X-ray luminosities ranging from 10^{40} to 10^{45} erg s $^{-1}$. If such sources undertake fluctuations in the luminosity of one order of magnitude or more on a timescale shorter than the dust creation timescale⁹, a grain distribution skewed towards large grains and dominated by graphite particles would be produced at a distance $R \sim 10^{17} L_{46}$ cm from the ionizing source, where L_{46} is the [1 eV–100 keV] peak luminosity in units of 10^{46} erg s $^{-1}$. It is worth mentioning, however, that the grains with size as large as 1 μ m discussed by Maiolino et al. (2001b) could not be created, unless already present before the sublimation took place.

3. Time evolution of opacities in various environments

In this section we explore the time evolution of the opacities under an intense X-ray UV radiation field in various types of environments, characterized by different types of dust distributions and various fractions of Hydrogen in its molecular form, H₂. We show how the time evolution can be a diagnostics of these quantities. We adopt here (unless otherwise noted) an illuminating spectrum $L_\nu \propto \nu^{-\alpha}$, with $\alpha = 0.5$ and normalization as in §2.3. The dependence of the opacities on the spectrum have been discussed in Paper I.

⁹The time scale for metals to return from the gas to grow large grains has been estimated by Laor & Draine (1993) to be $\sim 3 \times 10^4 n_6^{-1} \Delta v_5^{-1}$ yr, where $n_6 \equiv n/10^6$ cm $^{-3}$ is the density of the region, and $\Delta v_5^{-1} \lesssim 50$ is the mean speed of metal ions relative to the grains.

3.1. Time-variable extinction and reddening for various grain distributions

As discussed in the Introduction, measurements of spectral reddening at one given time can yield similar results for Galactic-type grain distributions with a low dust-to-gas ratio f_d , and for grain distributions skewed towards larger grains but with an higher value of f_d . Here we show that this degeneracy in the interpretation of the observational results can be removed with early time/continuous monitoring of the opacity and reddening.

The behavior of the optical opacity in the V band, A_V , is shown in the top panel of Figure 5 for three different values of the dust-to-gas ratio, that is $f_d = 0.01 f_\odot$, $0.1 f_\odot$, and f_\odot . For the value $f_d = 0.01 f_\odot$, we adopted in the simulation a slope $\beta = 3.5$ and a maximum grain size $a_{\max} = 0.25\mu\text{m}$, as typical of our Galaxy. For the other two values of f_d we chose, for the corresponding simulation (and using the same value of a_{\max}), the slope β that yielded the same reddening of the model $\{f_d = 0.01 f_\odot, \beta = 3.5\}$. In all cases, the region has density $n = 10^3 \text{ cm}^{-3}$ and radius $R = 10^{19} \text{ cm}$. For an observer that were to infer the values of f_d and β based on reddening, the three physical situations would be degenerate and not distinguishable on an observational basis. However, as Figure 5 shows, the time evolution of the opacity under the influence of an intense radiation field is different in the various scenarios. In particular, the opacity evolves more rapidly for steeper distributions. This is due to the fact that smaller grains are sublimated more easily (see e.g. Paper I).

The time evolution of the reddening, E_{B-V} , for the same values of $\{f_d, \beta\}$ is shown in the bottom panel of Figure 5. What is interesting to note here is the fact that, while A_V evolves more rapidly for *steeper* grain distributions, E_{B-V} evolves more rapidly for *shallow* grain distributions. To understand why this is so, one needs to look at Figure 2 which shows the behavior of $A_V(\beta)$ and $E_{B-V}(\beta)$. While $A_V(\beta)$ is almost insensitive to β (for the $a_{\max} = 0.25\mu\text{m}$ case that we have assumed here), $E_{B-V}(\beta)$ is a very sensitive function of β , and in particular it varies more and more rapidly as β decreases. This has the implication that, while the time-variable behaviour of $A_V(t)$ is essentially determined by the fact that the distribution with larger β evolves more rapidly (because of the more efficient destruction of the smaller grains), the behaviour of $E_{B-V}(t)$ is dominated by the fact that E_{B-V} decreases much more rapidly with β for smaller β .

The trend in the time evolution of the V-band extinction and reddening for different slopes of the initial grain distribution discussed above (for a region of density $n = 10^3 \text{ cm}^{-3}$ and radius $R = 10^{19} \text{ cm}$), still remains for a larger but less dense region (characterized by the same column density $N_H = 10^{22} \text{ cm}^{-2}$). This is shown in Figure 6, where the region is characterized by a lower density $n = 10^2 \text{ cm}^{-3}$ but larger radius $R = 10^{20} \text{ cm}$. The overall rate of time variation is however smaller due to the reduction in the flux at the larger radii.

It should be noted that, for a given spectrum¹⁰, there is a certain degree of degeneracy (in

¹⁰The degree of time variability due to dust destruction also depends on the spectral index of the illuminating

the observed time-variability in a given band) between the size/density of the region which is being illuminated and the spectral slope of the dust-grain distribution in the region. However, this degeneracy can be broken by measurements of time variability in both the optical and the X-ray band. In fact, while the former is mostly (but not only) governed by the process of dust destruction, the latter is mostly (but, again, not only; see Paper III), governed by the process of photoionization of the metals. And it should also be reminded that, as a result of the simultaneous processes of dust destruction and metal photoionization, the dust-to-gas ratio that is inferred from a comparison between the optical and X-ray extinction is most likely not reflecting the intrinsic properties of the region (see Paper I for a detailed discussion of this issue).

Figure 7 shows the time dependence of the V-band extinction and B-V reddening for grain size distributions with the same slope $\beta = 3.5$ but different values of the maximum size a_{\max} of the grains in the distribution. In all cases, the region has a density $n = 10^3 \text{ cm}^{-3}$ and radius $R = 10^{19} \text{ cm}$ with a solar value for the dust-to-gas ratio. Both the V-band extinction and the reddening evolve more slowly for grain distributions with larger a_{\max} , due to the longer sublimation time of the larger grains (see Paper I).

It should be remarked that the results above have been given for a source of constant luminosity in the time interval $\{0, t\}$. In the case where the source is the prompt GRB emission then, if no monitoring of the optical opacities is made during the prompt phase, the extinction and reddening that an observer would measure in the later afterglow phase is what it is at the time at which the prompt X-ray UV flash ends. This has the implication that short bursts are less likely to affect their environments than long bursts. Therefore, if the long GRBs with detected optical counterparts are actually those which manage to evacuate a funnel in their dusty environment, as claimed by Reichart (2001b), then it will be more difficult to detect optical counterparts for short bursts. Another consideration is the fact that, if short bursts are associated with mergers of two compact objects, and occur in low-density environments (e.g. Bloom, Sigurdsson & Pols 1999; but see Perna & Belczynski 2002), then no variability should be observable for them with early-time monitoring of the opacities. These types of observations could therefore provide an independent diagnostics of whether the classes of long and short bursts are actually associated with two different types of progenitors.

3.2. Effects of the presence of H_2 on the time-variable extinction

The presence of molecular Hydrogen in a cloud can be revealed through the absorption signatures imprinted in the spectrum (due to vibrationally excited H_2) in the wavelength range $1110\text{\AA} < \lambda < 1705\text{\AA}$. A detailed computation of the transmission spectrum has been performed

radiation (see e.g. Paper I); however, the spectrum is a quantity that is measured independently and therefore it does not constitute an element of degeneracy for this type of observations.

by Draine & Hao (2002). What we are mainly interested in here is the effect of the presence of molecular Hydrogen on the time variable signatures discussed above produced by various dust distributions.

Hydrogen in molecular phase can alter the evolution of the dust destruction fronts essentially for two reasons. Firstly, the cross section to photoionize H_2 and H_2^+ is different than that of Hydrogen; therefore, unless the absorbing region is optically thin to H and H_2 , the propagating flux (which is also responsible for dust sublimation) will be modified differently depending on whether Hydrogen is in its atomic or molecular form. Second and most important, is the presence of the singly ionized molecular Hydrogen H_2^+ . It is generated by photoionization of H_2 , and it is destroyed by the processes of photoionization ($H_2^+ + h\nu \rightarrow 2H^+ + e^-$) and photodissociation ($H_2^+ + h\nu \rightarrow H^+ + H$). While both the cross section thresholds to photoionization of H_2 and H_2^+ are above that of Hydrogen, the cross section for the process of photodissociation of H_2^+ is given by

$$\sigma(E) = 2.7 \times 10^{-16} \text{ cm}^2 \left(\frac{E}{29 \text{ eV}} \right)^2 \left(1 - \frac{E}{29 \text{ eV}} \right)^6 \quad \text{for } E < 29 \text{ eV}, \quad (5)$$

where we have adopted the fit derived by Draine & Hao (2002) to the photodissociation cross section found by von Bush & Dunn (1972) after averaging over the H_2^+ vibrational distribution. It can be seen that the cross section in Eq. (5) gives a direct contribution to the opacity in the optical range.

Let us now assume that, at $t = 0$, all Hydrogen is in its molecular form with an initial density $n(H_2) = n_H/2$. As discussed above, the process of complete photoionization of H_2 passes through the intermediate state of H_2^+ . During the process of photoionization, this is formed in a rather thin layer behind the photoionization front of H_2 . Draine & Hao (2002) found in their simulations that the column density $N(H_2^+)$ quickly stabilizes at a constant value that is roughly independent of the density of the medium, while it depends on the hardness of the incident spectrum, being lower for softer spectra. Our simulations confirm their results. Figure 8 shows the contribution to the V band opacity (top panel) and to the B-V reddening (bottom panel) due to the H_2^+ column density. We show the results for various combinations of values of the medium density ($n_H = 10 \text{ cm}^{-3}$, $n_H = 10^2 \text{ cm}^{-3}$ and $n_H = 10^3 \text{ cm}^{-3}$) and of the spectrum hardness ($\alpha = 0.5$ and $\alpha = 1$). As it can be seen from the Figure (note that the time oscillations are due to numerical inaccuracies in traversing the radial zones), H_2^+ provides a roughly constant value to the opacities, that is approximately independent of the density of the region and that is lower for a softer spectrum.

If molecular Hydrogen is present in the absorbing region, then it will be possible to appreciate the time variability in the opacity due to dust destruction only if the dust opacity is larger (at $t = 0$ and for at least a fraction of the time during which dust destruction takes place) than the contribution to the opacity provided by H_2^+ . Figure 9 shows the regions in the parameter space $\{\beta, f_d\}$ of values of β, f_d such that the contribution to opacity and B-V reddening by dust at $t = 0$ is above the contribution due to H_2^+ . The shaded region in the Figure denotes the parameter space where both $A_V(t = 0)$ and $E_{B-V}(t = 0)$ due to dust are above the corresponding contributions due to H_2^+ .

If the H_2^+ contribution to the opacity is lower than that of dust, then the time variable signatures due to dust destruction can be more easily identified. The differences in the transmitted spectrum impinging on the dust grains, due to differences in the opacities of H and H_2 , affect only marginally the time evolution of the dust opacity. This is illustrated in Figure 10 which shows, for two types of initial dust distributions, a comparison between the time variability of the dust contribution to the V band extinction and reddening, when all Hydrogen is in its atomic phase and when all Hydrogen is in its molecular phase before the onset of the source.

4. Observational prospects for observing time-variability during GRBs

Time-variable extinction can be detected when dust is being destroyed on a timescale comparable to the observation time. In order for this to happen, a source with very high X-ray/UV/optical luminosity is needed. The radiation generated by the prompt GRB emission constitutes the best example known so far of such a high luminosity source.

Optical observations of GRB afterglows are now performed regularly, with a reaction time that is decreasing with time. The time variability that we have described, however, requires optical monitoring *during* the early prompt phase. This constraint cannot be overemphasized. In fact, even if the afterglow phase of a GRB can have a fluence comparable to the prompt emission in the UV and soft X-ray range, dust sublimation will take place almost only during the prompt phase. This is due to the fact that, since the temperature of a grain is due to the balance of an input term (the rate of UV photon absorption) and an output one (the thermal emission of the grain), what causes the sublimation is the luminous prompt phase rather than the long lasting afterglow phase. Such a constraint is not applicable for photoionization, which proceeds as a function of the fluence and not of the flux, and therefore is much easier to detect the evaporation of the soft X-ray column than that of dust in the afterglow of GRBs (see Paper 3 for a more thorough discussion). The IFE dust destruction process, on the other hand, is sensitive to the fluence and may be relevant also in the afterglow phase. Numerical simulations in IFE dominated situations (see Paper 3), suggest however that IFE can only marginally contribute to the dust destruction even for hard GRB spectra. This consideration allows us to suggest a test to asses the importance of CE fragmentation, which is not included in the code (being exclusive with IFE). If CEs take place, the X-ray flux of the afterglow has still enough ionizing photons to modify the dust distribution and column density. For this reason, should any evolution of the extinction or reddening be observed during the afterglow phase of GRBs, this should be ascribed to the effect of Coulomb explosions, which are more effective than IFE and sensitive to fluence. To date, such an effect has never been observed, even though better data are certainly to be awaited before firm conclusions can be drawn.

Monitoring of the burst optical-UV flux during the prompt phase will be possible with *Swift*, which is planned to be launched in 2003. The optical telescope on board *Swift* will in fact provide optical and UV photometry and spectra on a timescale on the order of a few tens of seconds after

the GRB trigger. In a few cases, the repointing of the optical telescope should be made in even less time. For a GRB at $z \sim 1$, the V band rest frame falls in the NIR. Therefore, for the studies that we have proposed here, particularly important are the planned robotic telescopes from the ground (e.g. the REM telescope, Zerbi et al. 2002), which will provide NIR photometry on the same short timescale as *Swift* for the optical band.

5. Summary

We have used the time-dependent photoionization code for a dusty medium, developed by Perna & Lazzati (2002), to study the observational signatures in the optical extinction due to the evolution of the dust distribution in the close environment of a source of intense radiation field. This is of relevance in several astrophysical contexts, such as AGNs, GRBs and, albeit at different scales, for star formation. We have shown that a strong X-ray UV/optical radiation field can significantly modify the dust properties in the close environment of the source. In particular, we have found that the dust grain distribution becomes significantly flatter as a result of the faster sublimation of the smaller grains. This has the important consequence that the characteristic dust “bump” at 2275 Å is highly depleted. The lack of such a feature has been noted both in observations of AGNs and GRBs. Another consequence of the interaction of the radiation field with the dusty medium is the preferential destruction of silicates with respect to graphite. This might help explain the observed depletion of silicates with respect to graphite in AGNs.

In the case of a very luminous source, time variability can be detected on a relatively short timescale. This is the case of GRB sources occurring in dense and compact regions. We have shown how early-time (e.g. during the prompt phase) monitoring of the optical opacities with *Swift* and *REM* can shed light on the type of dust (in particular with respect to its grain-size distribution) in the environment of GRBs. More specifically, we have shown how it allows to break the observational degeneracy as to whether a grey extinction is the result of a low dust-to-gas ratio or of a dust grain distribution that is skewed towards large grains. The observations that we have proposed here are particularly relevant in order to gain a fair knowledge of what the properties (such as metallicity and dust content) of high-redshift galaxies really are.

We thank Roberto Maiolino for insightful comments on our manuscript. RP thanks the Osservatorio Astronomico di Monte Porzio-Roma for its kind hospitality and financial support during the time that part of this work was carried out.

REFERENCES

- Amati, L. et al. 2000, *Science*, 290, 953
Böttcher M., Dermer C. D., Crider A. W., Liang E. P., 1999, *A&A*, 343, 111

- Bloom, J. S., Sigurdsson, S., & Pols, O. R. 1999, MNRAS, 305, 763
- Draine, B. T. & Hao, L. 2002, ApJ, 569, 780
- Draine, B. T., & Lee, M. H. 1984, ApJ, 285, 89
- Fruchter, A. S. et al. 1999, ApJ, 516, 683
- Fruchter, A., Krolik, J. H. & Rhoads, J. E. 2001, ApJ, 563, 597
- Galama, T. & Wijers, R. A. M. J. 2001, ApJ, 549, 209
- Kulkarni, S. R., et al., 1999, Nature, 398, 389
- Laor, A. & Draine, B. T. 1993, 402, 441
- Lazzati, D., & Perna, R., 2002, MNRAS, 330, 383
- Lazzati, D., Perna, R., & Ghisellini, G. 2001a, MNRAS, 325, L19
- Lazzati, D., Ghisellini, G., Amati, L., Frontera, F., Vietri, M., & Stella, L. 2001b, ApJ, 556, 471
- Maiolino, R., Marconi, A. & Oliva, E. 2001a, A&A, 365, 37
- Maiolino, R., Marconi, A., Salvati, M., Risaliti, G., Severgnini, P., Oliva, E., La franca, F., Vanzi, L. 2001b, A&A, 365, 28
- Mathis, J. S., Rumpl, W. & Nordsieck, K. H. 1977, ApJ, 217, 425
- Mirabal, N. et al. 2002, ApJ in press, astro-ph/0207009
- Perna, R. & Belczynski, K. 2002, ApJ, 570, 252
- Perna, R., & Lazzati, D., 2002, ApJ in press (astro-ph/0206445)
- Perna, R., & Loeb, A. 1998, ApJ, 501, 467
- Perna, R., Raymond, J., & Loeb, A. 2000, ApJ, 533, 658
- Reichart, D. 2001a, ApJ submitted, astro-ph/0107546
- Reichart, D. 2001b, ApJ, 553, 235
- Savaglio, S., Fall, M. S. & Fiore, F. 2002, ApJ submitted, astro-ph/0203154
- Stratta, G. et al. 2002, ApJ submitted
- von Bush, F. & Dunn, G. H. 1972, Phy. Rep A, 5, 1726
- Waxman, E.; Draine, B. T. 2000, ApJ, 537, 796
- Weingartner, J. C. & Murray, N. 2002, ApJ in press, astro-ph/0208123
- Zerbi, F. M. et al. 2001, Gamma-Ray Bursts in the Afterglow Era, Proceedings of the International workshop held in Rome, CNR headquarters, 17-20 October, 2000. Edited by Enrico Costa, Filippo Frontera, and Jens Hjorth. Berlin Heidelberg: Springer, 2001, p. 434., 434

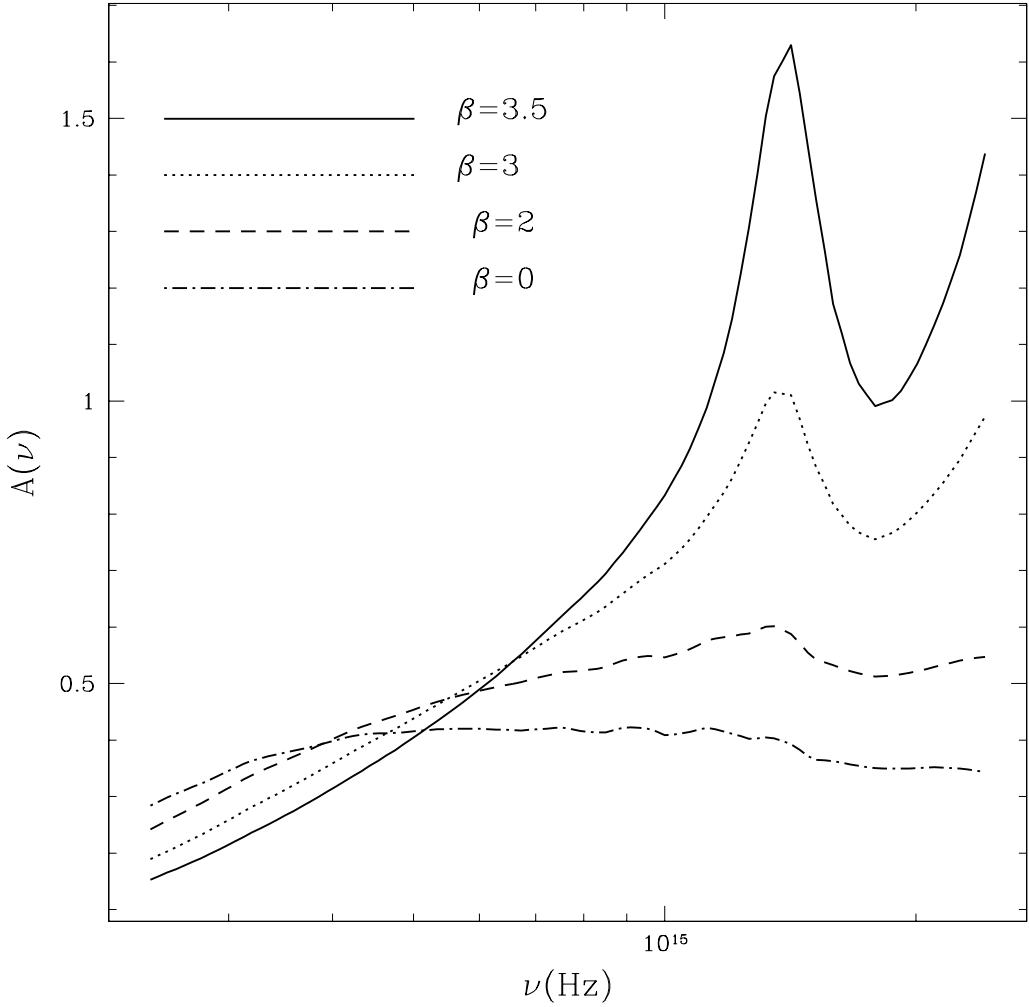


Fig. 1.— The extinction curve in the 1-10 eV energy range for power-law grain distributions of various slopes β and grains in the range $\{a_{\min} = 0.005\mu\text{m}, a_{\max} = 0.25\mu\text{m}\}$. The Hydrogen column density is $N_{\text{H}} = 10^{21} \text{ cm}^{-2}$ and the dust-to-gas ratio is $f_d = f_{\odot}$.

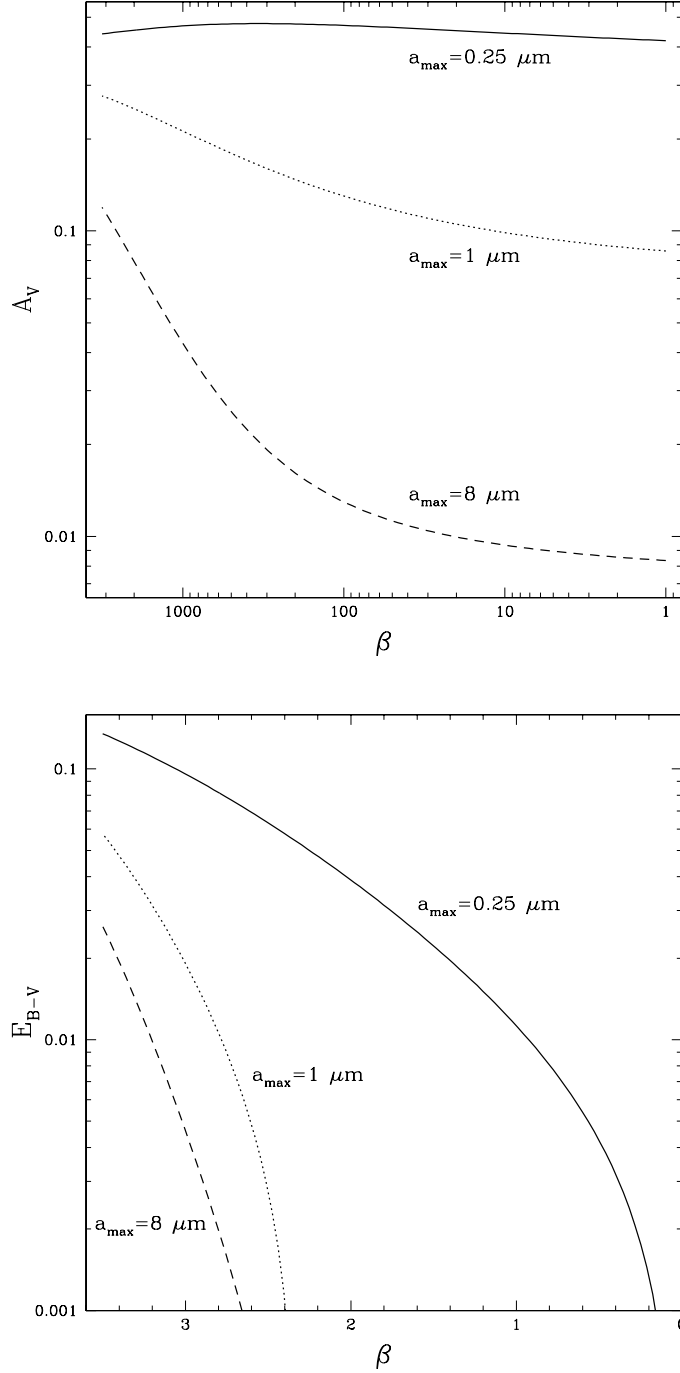


Fig. 2.— The V-band extinction (top panel) and the B-V reddening (bottom panel) are shown as a function of the power-law slope β of the grain distribution. The grains are in the range $\{a_{\min} = 0.005 \mu\text{m}, a_{\max} = 0.25 \mu\text{m}\}$. The Hydrogen column density is $N_{\text{H}} = 10^{21} \text{ cm}^{-2}$ and the dust-to-gas ratio is $f_d = f_{\odot}$.

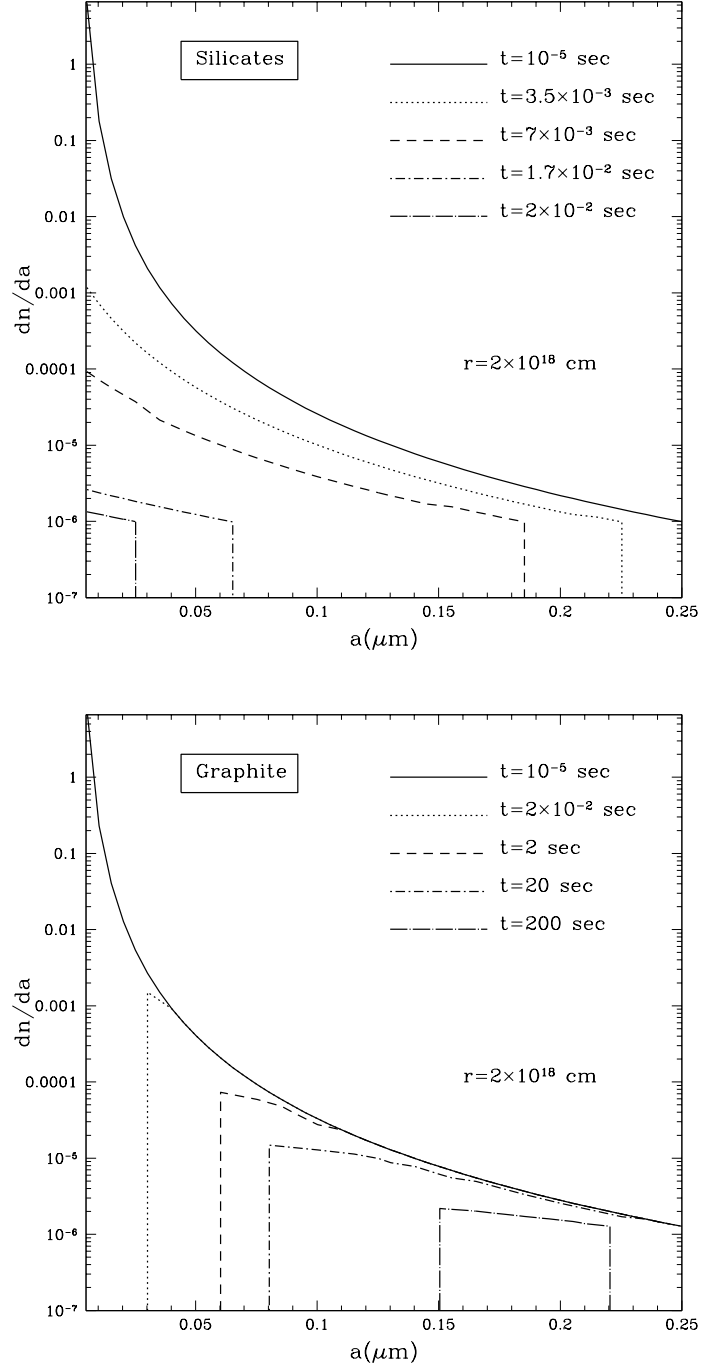


Fig. 3.— The evolution of the grain distribution at a distance $r = 2 \times 10^{18}$ cm from the source as the radiation flux impinges on the dust grains gradually reducing their sizes. The top panel shows the evolution for the silicates, while the bottom panel for graphite. Note that the silicates evolve much more rapidly than graphite.

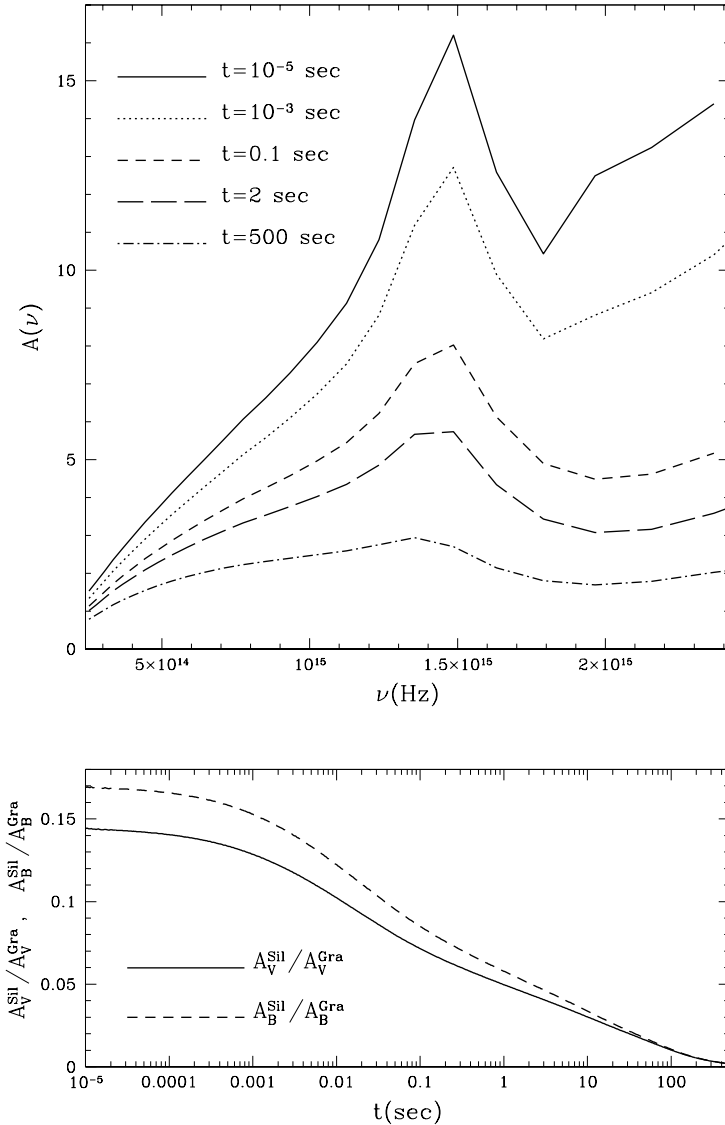


Fig. 4.— Top panel: the evolution of the extinction curve in a region of size $R = 10^{19}$ cm and density $n = 10^3$ cm $^{-3}$, as the radiation flux passes through it, altering the grain distribution. At $t = 0$ the dust mass fraction in silicates and graphite is assumed to be as for Galactic-type dust, but the bottom panel shows that the contribution of graphite with respect to silicates increases as the radiation flux impinges on the grains.

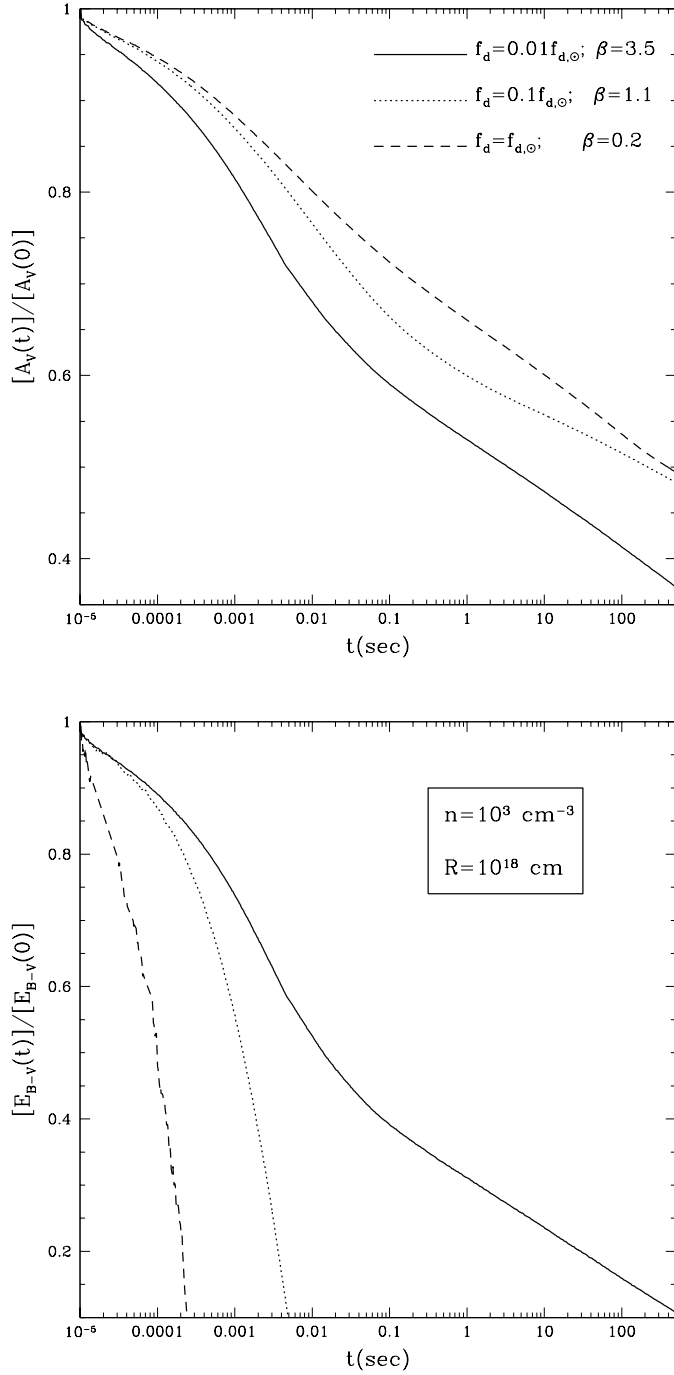


Fig. 5.— The behaviour of the extinction in the V band (top panel), and reddening E_{B-V} (bottom panel) under an intense X-ray UV radiation field, is shown for various slopes β of the grain distribution and different values of the dust-to-gas ratio f_d . The adopted values of $\{f_d, \beta\}$ are such that they yield the same reddening (before the source turns on). Note that the *steeper* the grain distribution, the higher the degree of variability of the optical extinction, while the *shallow* the grain distribution, the higher the degree of variability of the reddening.

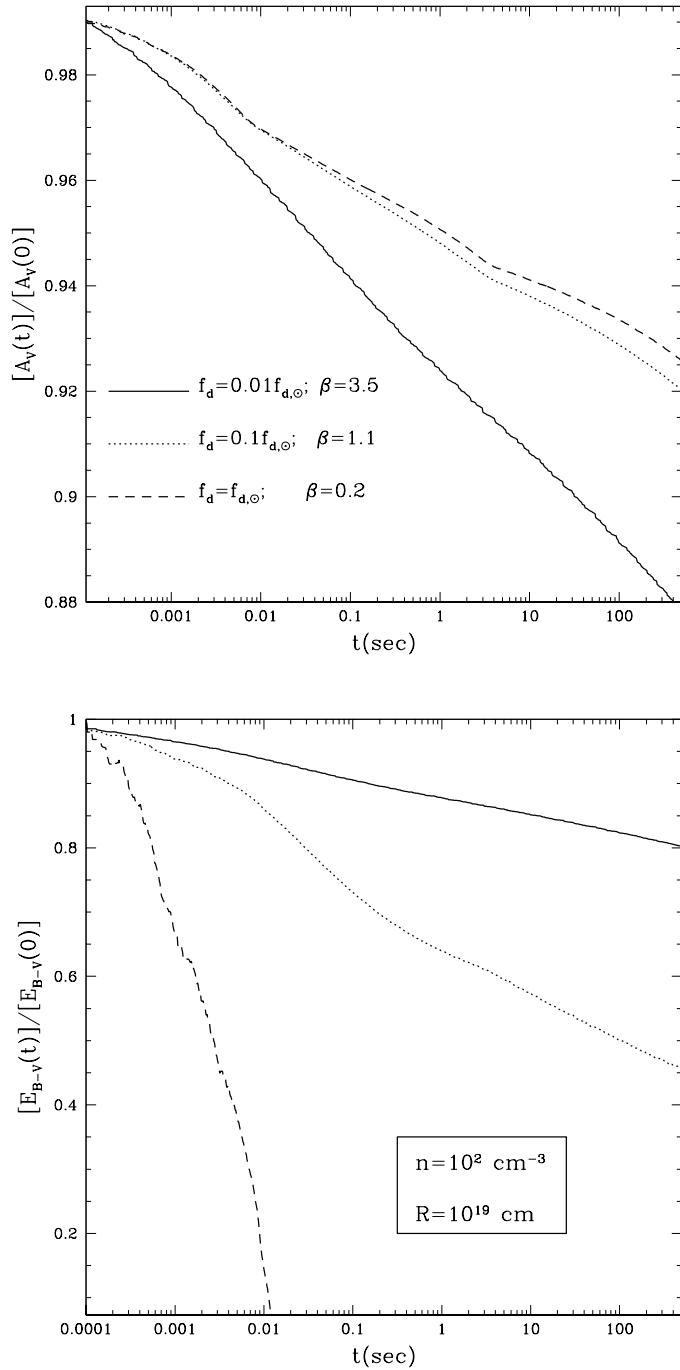


Fig. 6.— Same as in Fig. 5, but for a larger and less dense region.

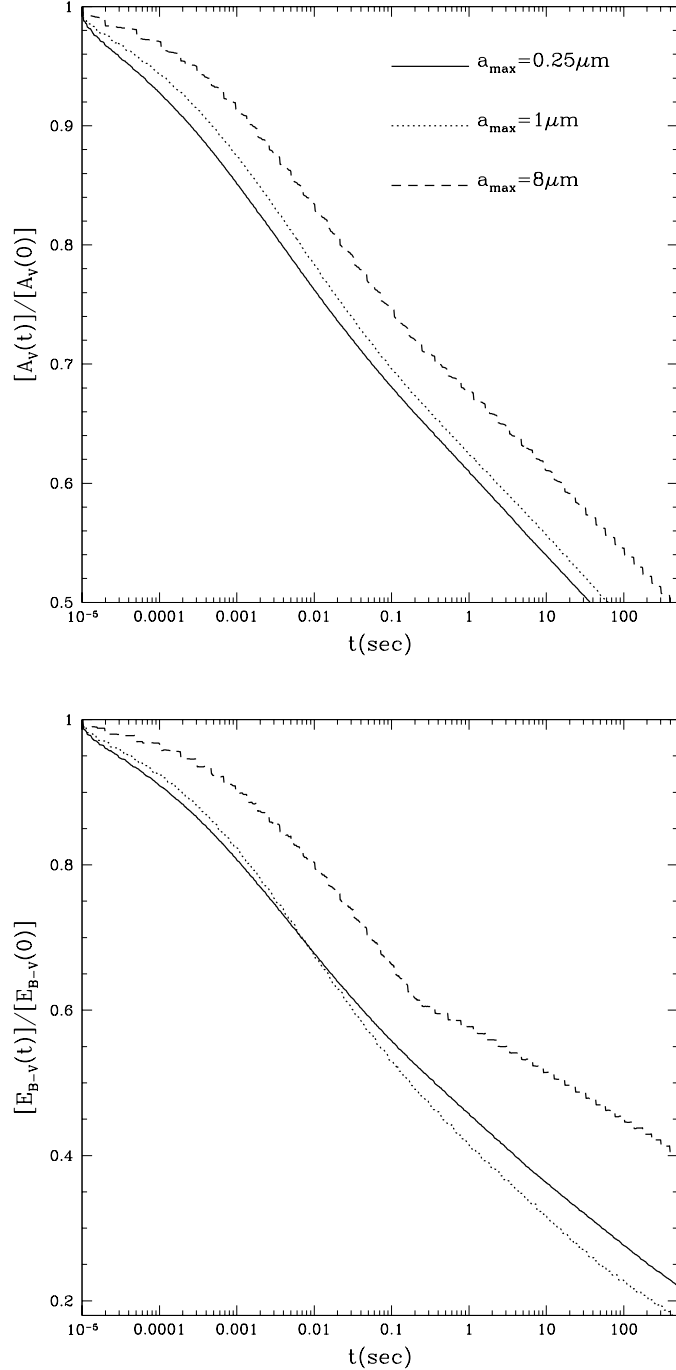


Fig. 7.— The behaviour of the extinction in the V band (top panel), and reddening E_{B-V} (bottom panel) under the X-ray UV radiation field, is shown here for various values of the largest grain a_{\max} of the initial dust grain distribution, and for the same value $\beta = 3.5$ of the slope of the distribution.

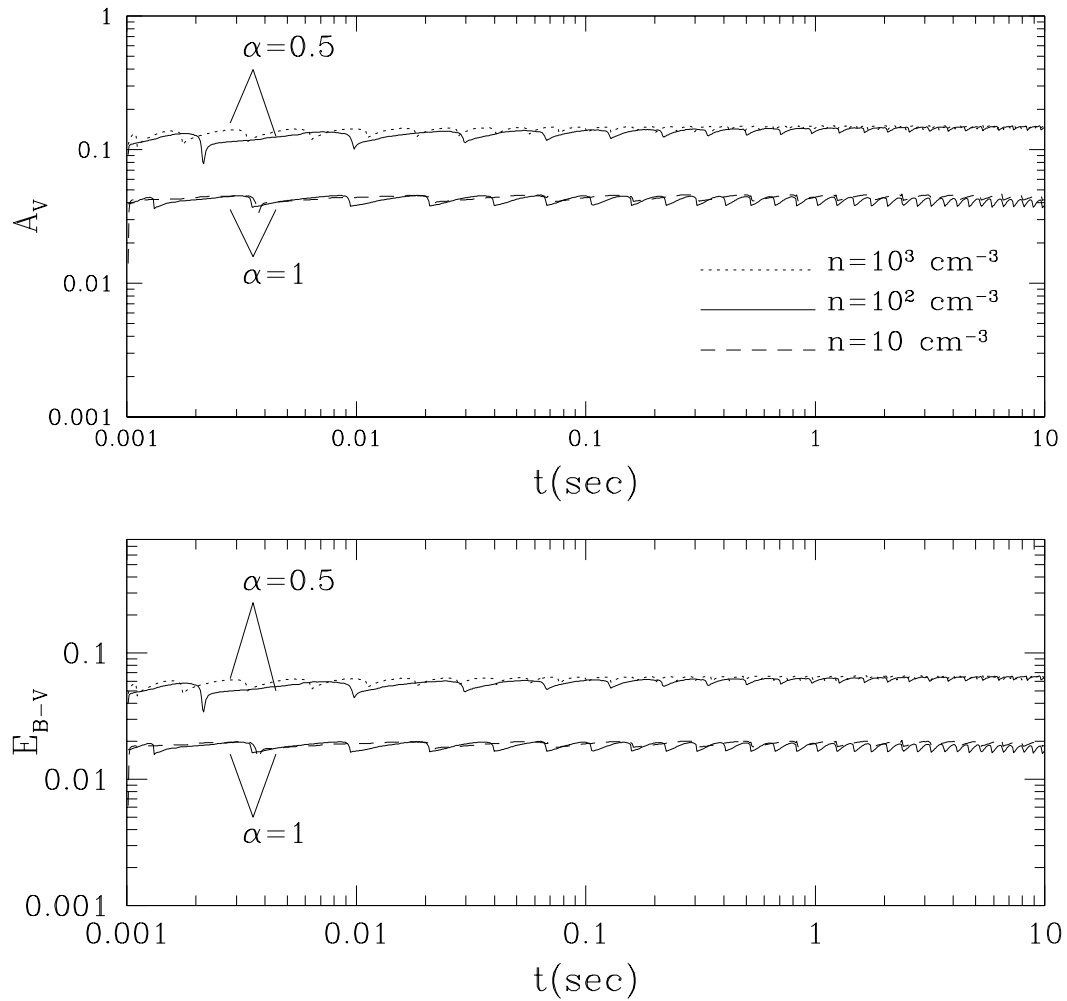


Fig. 8.— The contribution to the V-band opacity and the B-V reddening due to the process of photodissociation of H_2^+ . The oscillations are due to numerical inaccuracy in traversing radial shells.

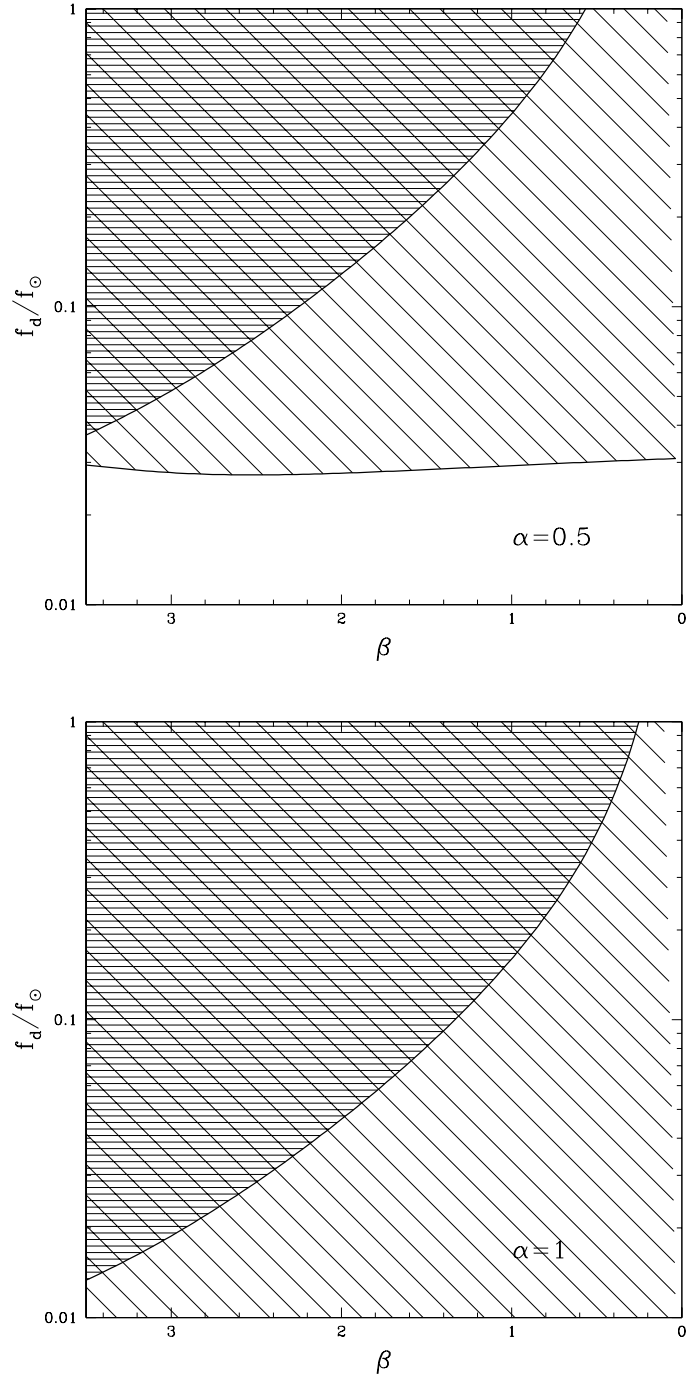


Fig. 9.— The shaded area marks the region in the parameter space of $\{\beta, f_d\}$ for which both the initial V-band opacity, $A_V^{\text{dust}}(0)$, and reddening, $E_{B-V}^{\text{dust}}(0)$, of dust (for a region whose Hydrogen column density is $N_H = 10^{22} \text{ cm}^{-2}$) are higher than the contribution due to H_2^+ . The dashed area in between the two lines marks the region where $A_V^{\text{dust}}(0) > A_V(H_2^+)$ but $E_{B-V}^{\text{dust}}(0) < E_{B-V}(H_2^+)$.

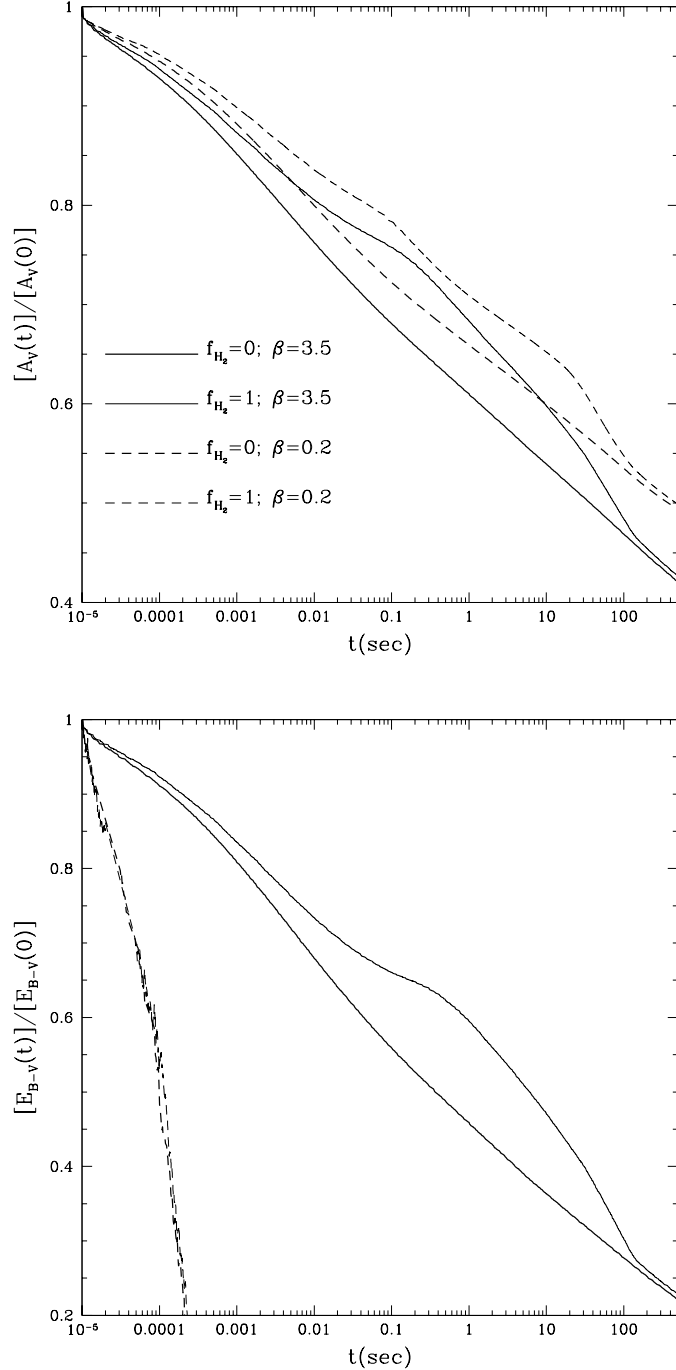


Fig. 10.— Comparison between the time evolution of the dust opacity and reddening when all Hydrogen is initially in its atomic phase and when it is all in its molecular phase. Here f_{H_2} represents the fraction of Hydrogen that is in molecular form.